

## DEFORMATION EFFECTS IN NEUTRON SCATTERING FROM THE Sm ISOTOPES

M.T. McEllistrem<sup>†</sup>, J. Lachkar, G. Haouat, Ch. Lagrange,Y. Patin, R.E. Shamu<sup>††</sup>, J. Sigaud and F. Coqu

Service de Physique Nucléaire - Centre d'Etudes de Bruyères-le-Châtel

B.P. n° 61 - 92120 Montrouge, France.

1 W 18

Deformation effects in neutron scattering from isotopically enriched  $\text{Sm}_2\text{O}_3$  samples have been studied at an incident neutron energy of 7 MeV where a maximum of the deformation effects was observed in total cross section measurements on the same isotopes.

Differential cross sections for elastic scattering and inelastic scattering (first  $2^+$  state) were measured for  $^{148}\text{Sm}$  and  $^{150}\text{Sm}$  and for  $^{146}\text{Nd}$ , which was included in this study to aid in separating isospin effects from deformation effects. Cross sections for the sum of elastic and inelastic scattering (first  $2^+$  state) were determined for  $^{152}\text{Sm}$  and  $^{154}\text{Sm}$ .

Experimental cross sections are compared to the results of non-spherical optical-potential coupled-channel calculations. ~~Calculated~~

(NUCLEAR REACTIONS  $^{146}\text{Nd}(n,n)$ ,  $(n,n')$ ,  $^{148,150}\text{Sm}(n,n)$ ,  $(n,n')$ ,  $^{152,154}\text{Sm}(n,n+n')$ ,  $E = 7.0$  MeV; measured  $\sigma(\sigma)$ ; calculated  $\leq (6)$ .)

Introduction

The results of several recent experiments suggest that the effect of nuclear deformation on fast neutron elastic and inelastic scattering may be appreciable. Holmqvist et al. have measured the angular distribution of neutrons elastically scattered from the deformed nucleus  $^{181}\text{Ta}$  between 2.5 and 8.0 MeV neutron energy.<sup>1</sup> The angular distribution at angles greater than about  $60^\circ$  was observed to be considerably damped, as compared to optical model fits to the data using a spherical potential.

Angular distributions computed using a non-spherical potential were found to provide significantly better fits to the data. Tanaka et al. have performed somewhat similar studies on natural isotopic mixtures of each of the elements Er and Gd over the neutron energy range 1.5 to 3.5 MeV.<sup>2</sup>

From the results of coupled channel calculations, i.e., by Tamura<sup>3</sup>, it is expected that nuclear deformation would have a strong effect on neutron inelastic scattering from both dynamically deformed and permanently deformed nuclei, that is, vibrational and rotational nuclei. As an extreme example, in the DWBA the direct part of the inelastic scattering is proportional to the square of the deformation parameter. Using a vibrational optical model, Fu and Perey have obtained good fits to inelastic scattering data on Pb for 14 MeV incident neutrons.<sup>4</sup> Also, Belovitzk et al.<sup>5</sup> have studied the excitation by 14 MeV neutrons of the low-lying octupole states of the isotopes  $^{206,207,208}\text{Pb}$ . In this latter work reasonable agreement between the experimental data and the results of calculations based on DWBA theory was found. We are not aware of any published cross sections on neutron inelastic scattering, separated from the elastic scattering, for heavy, permanently deformed nuclei at incident neutron energies where direct excitation of the rotational levels predominates.

In the present work, deformation effects in neutron scattering were investigated by scattering 7 MeV neutrons from the isotopes  $^{148}\text{Sm}$ ,  $^{150}\text{Sm}$ ,  $^{152}\text{Sm}$ , and  $^{154}\text{Sm}$ . The Sm isotopes are desirable nuclei for studying the effects of nuclear deformation because they span the region near  $N = 88$  where the nuclear deformation changes rapidly. In this regard the nucleus  $^{150}\text{Sm}$  is of special interest because of its role as a transitional nucleus between vibrational and rotational nuclei. The nucleus  $^{146}\text{Nd}$  was included in these investigations, also, in order to separate possible isospin effects from deformation effects. The Sm and Nd samples were isotopically enriched and were available only in the form of oxides.

Differential cross sections for elastic scattering and inelastic scattering to the first  $2^+$  state were measured for the nuclei  $^{146}\text{Nd}$ ,  $^{148}\text{Sm}$ ,  $^{150}\text{Sm}$ ;

whereas for  $^{152}\text{Sm}$  and  $^{154}\text{Sm}$ , cross sections for the sum of elastic and inelastic scattering (first  $2^+$  state) were determined. Measurements were performed over the angular range  $20^\circ$  to  $145^\circ$ ; however, inelastically scattered neutrons were not observed directly at forward angles because of appreciable elastic scattering from oxygen.

An incident energy of 7 MeV was chosen for the present study primarily because, as shown in fig. 1, measurements<sup>6</sup> and calculations<sup>7</sup> of total cross section differences for the Sm isotopes suggest that at this energy the deformation effects in neutron scattering may be maximum. Calculations using a range of deformation parameters indicate that the energy of this maximum does not depend appreciably on nuclear shape.<sup>7</sup> This incident energy is believed to be sufficiently high that compound elastic scattering effects are unimportant for these nuclei.

Experimental Method

The differential cross section measurements were performed using the neutron time-of-flight facility of the Centre d'Etudes de Bruyères-le-Châtel, which has been described in detail elsewhere.<sup>8</sup> Briefly, proton bursts of repetition rate 2.5 MHz and width 1 nsec (FWHM) were accelerated by the Bruyères tandem accelerator. Monoenergetic 7-MeV neutrons were produced by bombarding tritium, contained in a 3-cm long gas target at a pressure of about 1.5 atm, with this pulsed proton beam. Neutrons were scattered by cylindrical samples located at  $0^\circ$  with respect to the incident proton beam and 11.3 cm from the center of the gas target. The scattered neutrons were detected by an array of four detectors placed at  $20^\circ$  intervals, each detector consisting of a 12.5-cm diameter, 5-cm thick NE-213 liquid scintillator which was optically coupled to an XP-1040 photomultiplier tube. Pulse-shape discrimination was utilized to reject  $\gamma$ -ray induced events in the scintillators. The data acquisition system which was employed permitted off-line adjustment of the energy threshold for neutron detection. Only scintillation pulses which corresponded to neutron energies greater than 1.5 MeV were utilized in the present work.

Each neutron detector was housed in a shield consisting of polyethylene and lead and was placed behind a 1.5 m collimator composed of paraffin loaded with lithium and boron. Four 70-cm long Fe shadow bars with W tips were positioned near the gas target in order to reduce background caused by direct neutrons. The flight path from the sample to each detector was 8 m. For this flight path the energy spreads and time spreads of the experiment were such that the overall energy spread at each neutron detector was less than 150 keV. With this spread, kinematic

NOTICE

PORTIONS OF THIS REPORT ARE ILLEGIBLE. It has been reproduced from the best available copy to permit the broadest possible availability.

MASTER

DISTRIBUTION OF THIS DOCUMENT UNLIMITED

1

fay

## **DISCLAIMER**

**Portions of this document may be illegible in electronic image products. Images are produced from the best available original document.**

separation of the oxygen scattering was sufficient to observe the inelastic scattering to first excited states for  $^{146}\text{Nd}$  and  $^{148,150}\text{Sm}$  at angles  $\geq 90^\circ$ .

Detector efficiencies were determined by scattering neutrons from a 1-cm diameter 4-cm high polyethylene sample and by counting directly monoenergetic neutrons from the  $D(d,n)$  reaction.<sup>9</sup> The incident neutron flux was measured using a proton-recoil counter telescope.

The number of incident neutrons from the gas target was monitored by an auxiliary NE-213 liquid scintillation detector placed at  $55^\circ$  to the incident proton beam and about 10 m from the gas target.

All samples were contained in air-tight thin-walled polyethylene cans about 2.2 cm in diameter and 5 cm high. The Sm samples,  $^{148,150,152,154}\text{Sm}$ , consisted of powdered  $\text{Sm}_2\text{O}_3$  and ranged in mass from 40.8 g ( $^{154}\text{Sm}_2\text{O}_3$ ) to 68.6 g ( $^{148}\text{Sm}_2\text{O}_3$ ). The isotopic enrichment of each sample was greater than 96% except for  $^{150}\text{Sm}$ , for which the enrichment was 87.4%. The  $^{146}\text{Nd}_2\text{O}_3$  sample had a mass of 63.6 g and an enrichment of 94.5%.

Background peaks in the TOF spectrum caused by the carbon of the polyethylene can and the oxygen of the oxide samples were subtracted with the aid of an empty can and an  $\text{H}_2\text{O}$  sample, respectively.

Cross sections were corrected for neutron flux attenuation in the sample, multiple scattering, and geometrical effects using the analytic method described by Kinney.<sup>10</sup>

### Results and Discussion

Some of the results from a preliminary analysis of the data are given in figs. 2, 3 and 4.

The measured differential cross sections for elastic scattering are presented in fig. 2 for each of the nuclei  $^{146}\text{Nd}$ ,  $^{148}\text{Sm}$ , and  $^{150}\text{Sm}$ . The uncertainty of each datum has been estimated to be about the size of the data point or smaller, except at  $35^\circ$  where the statistical uncertainty is about 12% because the  $^{160}$  scattering is relatively large at that angle. It is observed that the three angular distributions are very similar. Quantitative comparisons were made by making a Legendre fit to each distribution. The Legendre curves for  $^{148}\text{Sm}$  and  $^{150}\text{Sm}$  for example, were found to differ by at most about 10% over the angular range of the measurements. Also shown in this figure is the result of a coupled channel calculation for  $^{148}\text{Sm}$ , which was assumed to be a vibrational nucleus with a quadrupole deformability,  $\beta_2$ , of 0.13. The deformed-potential optical-model parameters which were used for this calculation were determined by fitting total cross section data,<sup>11</sup> strength function data, and potential scattering at low energies. These parameters are similar to parameter set 2 of ref. 7. It is seen that the agreement between the experimental and calculated cross sections for  $^{148}\text{Sm}$  is remarkably good, even though no attempt has been made to fit the present data.

The cross section data for  $^{152}\text{Sm}$  and  $^{154}\text{Sm}$  are given in fig. 3. For each of these nuclei, the cross sections for the sum of elastic scattering plus inelastic scattering to the first excited state are shown. Here, also, the experimental uncertainties are about the size of the data points or smaller, except at  $35^\circ$ . It is observed that the angular distributions for these two nuclei are very similar, except for small differences at the  $40^\circ$  and  $80^\circ$  minima and at angles greater than  $120^\circ$ . The calculated curve for  $^{154}\text{Sm}$  given in this figure represents the sum of cross sections for elastic plus inelastic (first  $2^+$  state) scattering. This coupled-channel calculation differed from the one for  $^{148}\text{Sm}$  in that: 1)  $^{154}\text{Sm}$  was assumed to be a rotational nucleus, 2) the real part of the optical potential was about 1% smaller in magnitude

for  $^{154}\text{Sm}$  because of the inclusion of an isospin term in the optical potential, and 3) the quadrupole deformation was taken to be 0.22. The parameters used for the  $^{148}\text{Sm}$  and  $^{154}\text{Sm}$  calculations provide a very good fit to total cross section difference measurements<sup>11</sup> over the energy range 1 to 15 MeV. These parameters have not been adjusted in order to improve the fit to the  $^{154}\text{Sm}$  data of the present work. Again, it is seen that there is good agreement between the calculated curve and the data.

Figure 4 shows a comparison of elastic scattering angular distributions between the vibrational nucleus  $^{148}\text{Sm}$  and the rotational nucleus  $^{154}\text{Sm}$ . For  $^{148}\text{Sm}$ , the cross section data and calculated curve presented here are identical to those given in fig. 2. The elastic cross sections for  $^{154}\text{Sm}$  were obtained by subtracting the computed inelastic ( $2^+$ ) cross sections from the experimental ( $0^+ + 2^+$ ) cross sections. The  $^{154}\text{Sm}$  calculated curve in this figure represents, of course, only elastic scattering.

No inelastic cross sections will be presented in the present report, primarily because of space limitations. It suffices to say at this time that at backward angles the inelastic cross sections for scattering to the first  $2^+$  state are similar for  $^{146}\text{Nd}$  and  $^{148}\text{Sm}$  and significantly larger for  $^{150}\text{Sm}$  as compared to the two lighter nuclei.

It was possible for each of the nuclei studied to compare the  $0^\circ$  differential cross section, determined by means of a Legendre fit, with Wick's limit, since measured total cross section values are available at 7.0 MeV for these Sm isotopes<sup>11</sup> and the  $^{146}\text{Nd}$  nucleus.<sup>12</sup> The differences ranged from 16% for  $^{148}\text{Sm}$  to -6% for  $^{154}\text{Sm}$  with a standard deviation of 4%. This standard deviation is well within the range expected on the basis of the estimated uncertainties for the present work and for the total cross section measurements.

The elastic differential cross sections for  $^{148}\text{Sm}$  and the elastic plus inelastic differential cross sections for  $^{154}\text{Sm}$  of the present work at 7.0 MeV have been compared to the results of recent measurements on these nuclei at 6.25 MeV neutron energy which were performed at the TOF facility of the University of Kentucky.<sup>13</sup> For each isotope the angular distributions at the two energies were observed to be in good qualitative agreement. Coupled-channel calculations indicated that the small quantitative differences which were present were a consequence of the different energies which were employed.

The work of Holmqvist et al.<sup>1</sup> on  $^{181}\text{Ta}$  suggests that the major effect of nuclear deformation on the elastic scattering of neutrons is to increase considerably the cross sections at the minima of the elastic angular distributions. However, the data and the calculated curves presented in fig. 4 indicate that for the Sm isotopes the effect of an increased quadrupole deformation parameter is to lower the elastic scattering angular distribution at back angles.

The reason for this apparent difference in deformation effects between Ta and Sm is not clear at the present time. Holmqvist et al. assumed that inelastic scattering to the 6 keV state of  $^{181}\text{Ta}$ , which of course was not experimentally resolved, was negligible. However, the 6.25 MeV study<sup>13</sup> of Sm, the present work, and coupled-channel calculations<sup>3</sup> for the scattering of 17.5 MeV neutrons by  $^{156}\text{Gd}$  all indicate that for even-A deformed rare earth nuclei, inelastic scattering to the first excited state is larger than elastic scattering at most back angles. Thus, contrary to their assumption<sup>1</sup>, it is likely that inelastic scattering to the 6 keV state of  $^{181}\text{Ta}$  is relatively very large, also.

### Acknowledgements

It is a pleasure to thank Dr. A. Michaudon for his support and encouragement, Jean Sol and his group for dehydrating and compacting samples, and the USAEC for the loan of the samples.

### References

- \* present address : University of Ky., Lexington, Ky.
- \* On leave from West. Mich. Univ., Kalamazoo, Mich.
- 1. B. Holmqvist, T. Wiedling, V. Benzi, L. Zuffi, *Nucl. Phys.* A150, 105 (1970).
- 2. S. Tamaka, Y. Tomita, Y. Yamanouti, K. Ideno, *Nuclear Structure Study with Neutrons* (Plenum Press N.Y., 1974) p. 148.
- 3. T. Tamura, *Rev. Mod. Phys.* 37, 679 (1965).
- 4. C.Y. Fu and F.G. Perey, *ORNL - 47* (1972).
- 5. G. Belevitzk, L. Kolesnikova, I. Frank, *Nuclear Structure Study with Neutrons* (Plenum Press, N.Y., 1974) p. 166.
- 6. Shamu, Bernstein, Blondin, Ramirez, Rochau, *Phys. Lett.* 45B, 241 (1973).
- 7. Ch. Lagrange, *Lett. J. de Phys.* 35, 111 (1974).
- 8. Haouat, Lachkar, Patin, Sigaud, Coqu, C.E.A. R-4641 (1975).
- 9. H. Liskien and A. Paulsen, *Nucl. Data Tables* 11, 569 (1973).
- 10. W.E. Kinney, *Nucl. Inst. Meth.* 83, 15 (1970).
- 11. R. Shamu, E. Bernstein, J. Ramirez, *Bull. Am. Phys. Soc.* 19, 103 (1974).
- 12. E. Bernstein and R. Shamu, *private communication*.
- 13. Burrows, Dawson, Glasgow, Hardie, Lagrange, McDaniel, *private communication*.

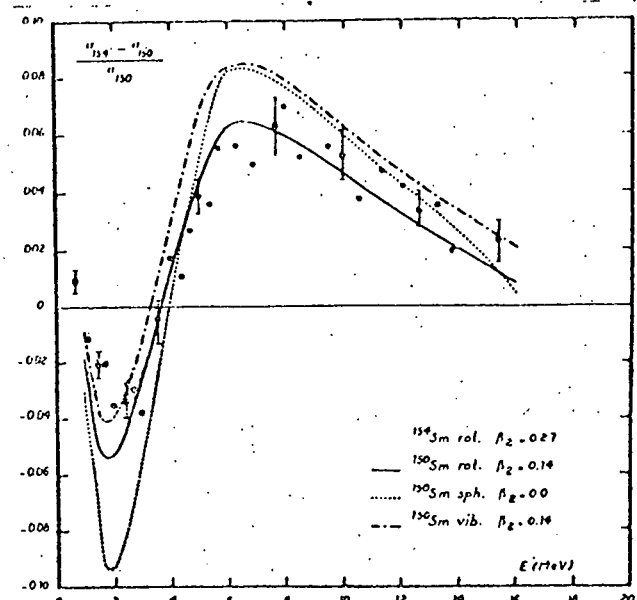


Fig. 1. Variation with neutron energy of the relative difference between the total cross sections<sup>6</sup> of <sup>154</sup>Sm and <sup>150</sup>Sm. The curves are the results of coupled-channel calculations<sup>7</sup>.

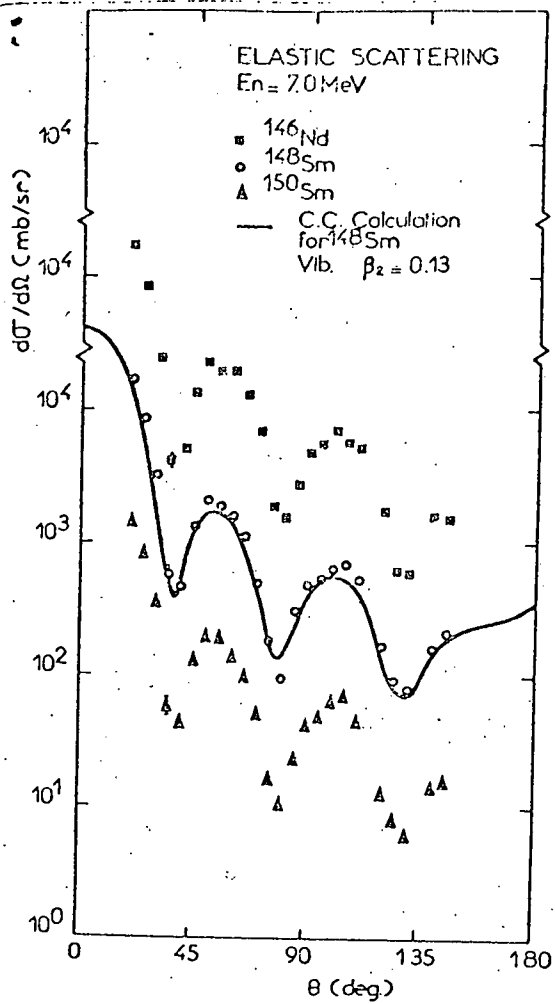


Fig. 2 (above) Elastic scattering angular distributions for  $^{146}\text{Nd}$ ,  $^{148}\text{Sm}$  and  $^{150}\text{Sm}$  at 7.0 MeV incident neutron energy. The solid line is the result of a coupled-channel calculation for  $^{148}\text{Sm}$ .

Fig. 3 (topright) Angular distributions for the sum of elastic and inelastic (first  $2^+$  state) cross sections for  $^{152}\text{Sm}$  and  $^{154}\text{Sm}$  at 7.0 MeV incident neutron energy. The solid line represents the calculated cross sections for elastic and inelastic (first  $2^+$  state) scattering by  $^{154}\text{Sm}$ .

Fig. 4 (bottom right) Comparison of elastic scattering angular distributions between  $^{148}\text{Sm}$  (vibrational nucleus) and  $^{154}\text{Sm}$  (rotational nucleus). The data points for  $^{154}\text{Sm}$  represent the difference between the experimental ( $0^+ + 2^+$ ) and the computed inelastic ( $2^+$ ) cross sections. The solid lines are calculated elastic angular distributions.

